

Phototransistors of Engineered InGaZnO Channel for Specific Molecular Detection in the Visible Range

Yupeng Yang, Mohammad Hadi Khaksaran, Jong Bin An, Sujin Lee, Hyun Jae Kim, Ted Johansson, Xi Lu, Ilya Sychugov, Apurba Dev, and Shi-Li Zhang*




Cite This: *ACS Appl. Opt. Mater.* 2024, 2, 2092–2100



Read Online

ACCESS |

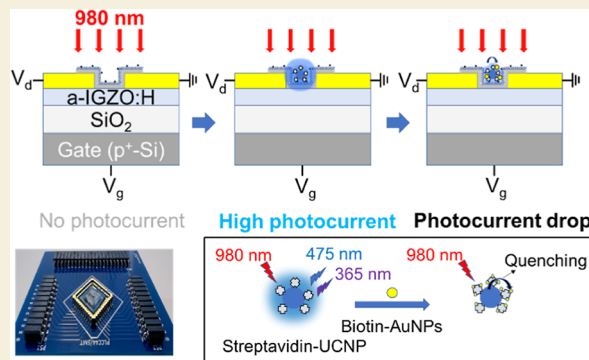
 Metrics & More

 Article Recommendations

 Supporting Information

ABSTRACT: Fluorescence-based single-molecule detection has been widely investigated and applied in biosensing and bioimaging due to its ultrahigh sensitivity and specificity. However, bulky and expensive commercial fluorescence microscopes are usually required. The Stokes shift property of most commonly used fluorophores requires optical sets such as dichroic mirrors and specific filters in the optical pathway before a photodetector to eliminate excitation and scattering lights from the fluorescence signals. The fluorescence signal collected by an objective is further unavoidably attenuated, and the optical resolution is diffraction-limited. Herein, a proof of concept of a lab-on-a-chip compatible molecular sensor is shown by integrating upconversion nanoparticles (UCNPs) and amorphous hydrogen-doped InGaZnO (InGaZnO:H) thin-film phototransistor (IGZO:H TFTs) aiming to alleviate those issues. Upon illumination with a 980 nm infrared light, the phototransistor shows no photocurrent without UCNPs but yields a high photocurrent with UV–visible fluorescent light emitted from the UCNPs. The molecular detection is enabled by further involving the Förster resonance energy transfer (FRET) mechanism, with the UCNPs as donors. The photocurrent falls back to its original low level when biotinylated gold nanoparticles are added to selectively bind and quench the UCNPs via biotin–streptavidin coupling. Each UCNP shows an estimated photocurrent-to-dark current ratio of 10^3 and each biotinylated gold nanoparticle causes at least 1 order of magnitude decrease of the photocurrent. Our integrated setup presents a promising platform for further development toward an optoelectronic biosensor capable of single-molecule detection.

KEYWORDS: α -IGZO thin film, phototransistor, upconversion nanoparticles, Förster resonance energy transfer, specific biosensing



INTRODUCTION

Photodetectors such as photomultiplier tubes or charged-coupled device cameras in the visible light region have been widely adopted in fluorescence microscopes and spectrometers for biosensing and bioimaging. In these systems, the excitation light and scattering lights have higher photon energy than the emission fluorescence signal due to the inherent Stokes-shift (downconversion) property of most commonly used fluorophores. Consequently, achieving a high signal-to-noise ratio (SNR) necessitates the inclusion of objectives, dichroic mirrors, and specific filters in the optical path to eliminate excitation and scattering lights from the fluorescence signal. However, having these elements in the optical pathway, as well as the objective for collecting fluorescence signals, unavoidably leads to partial attenuation of the fluorescence signal and diffraction-limited optical resolution. Additionally, fluorescence microscopes or spectrometers are usually bulky, complicated, and expensive, needing a special installation environment and trained operators. To address these limitations and enable direct fluorescence signal detection with a photodetector,

utilization of fluorophores with the anti-Stokes shift (upconversion) property can be viable.

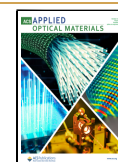
Upconversion nanoparticles (UCNPs) are unique fluorophores with a range of advantages, including anti-Stokes shift, high SNR, high photostability, good biocompatibility, and high penetration depth into tissues over other fluorophores like quantum dots, organic dyes, and fluorescent proteins.^{1–5} By name, UCNPs can absorb near-infrared (NIR) light and emit visible or even ultraviolet light due to the inherent ladder-like and metastable excited states. This unique feature of UCNPs makes them an ideal choice to be directly integrated with photodetectors for high SNR but without any other optical components. With this setup, the emitted visible light from UCNPs can generate photocurrents in the photodetectors,

Received: July 15, 2024

Revised: September 24, 2024

Accepted: September 26, 2024

Published: October 3, 2024



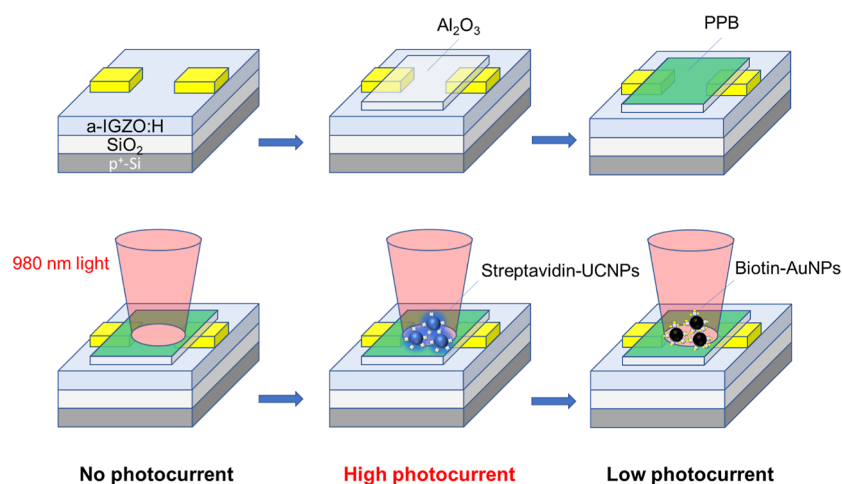


Figure 1. Concept of the integration of IGZO:H-TFTs with UCNP and FRET to realize sensitive and specific molecular detection. The SA-UCNPs are immobilized between the source and drain electrodes after surface functionalization. Changes in the photocurrent of the TFT are caused by the successive additions of SA-UCNPs and biotin-AuNPs.

while the NIR excitation light with lower energy than the band gap of the semiconductor channel of the photodetectors cannot activate the phototransistors. Moreover, the nonlinear optical process of UCNP can be excited at relatively low excitation power density of continuous-wave (CW) lasers, unlike the upconversion generated by simultaneous absorption of multiphotons requiring a high excitation power density from pulsed lasers.^{5–8}

A dense layer of UCNP has been combined with graphene,^{9,10} graphene/GaAs,¹¹ MoS₂,^{12–15} quantum dots,¹⁶ perovskites,^{17,18} carbon nanotubes,¹⁹ and silicon²⁰ photodetectors to extend their spectral response to the NIR region. But for highly sensitive and specific biosensing, only one UCNP is ideally needed per photodetector. Single UCNP-based biosensing for DNA, RNA, proteins, and biomarkers can be achieved via the Förster resonance energy transfer (FRET) mechanism.^{21,22} The FRET process describes the nonradiative energy transfer from a donor fluorophore to an acceptor fluorophore or a quencher to accomplish the sensing task; the efficiency of FRET is sensitively dependent on the spectral overlap, the amplitude of scalar product, and the distance (usually within 10 nm) between the donor and acceptor fluorophores, thereby enabling near-field optics. Thus, the fluorescence intensity change of the UCNP could indicate the analytes.

Phototransistors (TFTs) based on amorphous InGaZnO (α -IGZO) thin films with unique high and isotropic electron mobility (>10 cm² V⁻¹ s⁻¹) have been widely applied in biosensors, large-area display, memory, and neuromorphic electronics.^{22–32} As for sensor applications, α -IGZO TFTs have been explored as ion-sensitive field-effect transistors (ISFETs) or electrolyte-gated field-effect transistors.^{29–31} For such ISFET applications involving electrolytes, a bulky reference electrode is required.³³ Furthermore, ions as well as charges on DNA and protein molecules that lie beyond the so-called Debye length cannot be reproducibly detected by the ISFET method irrespective of the type of semiconductor channel used.³⁴ Concurrently, research interest in applying α -IGZO TFTs as phototransistors has sharply increased during the past decade.³² A phototransistor is immune to the Debye screening effect because it has optical input signals and electrical output signals. However, the wide band gap (>3.0

eV) of pristine α -IGZO films limits its absorption of visible lights. Recently, hydrogen plasma doping has been used to generate subgap states in the α -IGZO film, i.e., α -IGZO:H, to enable visible light detection and boost its electrical performance.^{35–39}

In this work, we demonstrate the proof of principle of an integrated biosensor based on the novel combination of (i) UCNP conjugated affinity probes, thus providing anti-Stokes shifted fluorescence, (ii) FRET-induced fluorescence quenching mediated by Au nanoparticles conjugated analyte, and (iii) phototransistors with submicron-sized source and drain contacts to an ultrathin α -IGZO:H film, i.e., IGZO:H-TFTs, to detect the fluorescence emission and the quenching signal from (i) and (ii), respectively. The detection is characterized by a high photocurrent-to-dark current ratio of 10^5 with about one hundred UCNP between the source and drain electrodes. The fabricated chip, each featuring an array of IGZO:H-TFTs, is wire-bonded and mounted onto a custom-designed printed circuit board (PCB) for optoelectronic measurements. Streptavidin-conjugated UCNP (SA-UCNP) are immobilized by simple drop-casting above the IGZO:H-TFT channel regions between the source and drain electrodes. Further, proof of concept biosensing is presented where a representative phototransistor successfully detects the FRET signal between the donor (SA-UCNP) and the quencher, i.e., biotinylated gold nanoparticles. This proof of concept integration of IGZO:H-TFTs, UCNP, and FRET is promising for the development of a sensitive, inexpensive, and portable optoelectronic biosensor platform for single-molecule detection. This integration intends to draw on the attractive features of α -IGZO films including large-area deposition capability at low temperatures, homogeneous and highly reproducible electronic properties, and direct-band gap nature with low dark current and high photocurrent efficiency.^{22–32}

RESULTS AND DISCUSSION

The working principle for specific molecular detection and the key steps of the concept are illustrated in Figure 1. After the fabrication of IGZO:H TFTs and surface functionalization, the SA-UCNPs are immobilized between the source and drain electrodes of the IGZO:H-TFTs. By biasing the IGZO:H-TFTs in their “OFF” state, the proof of concept is finally

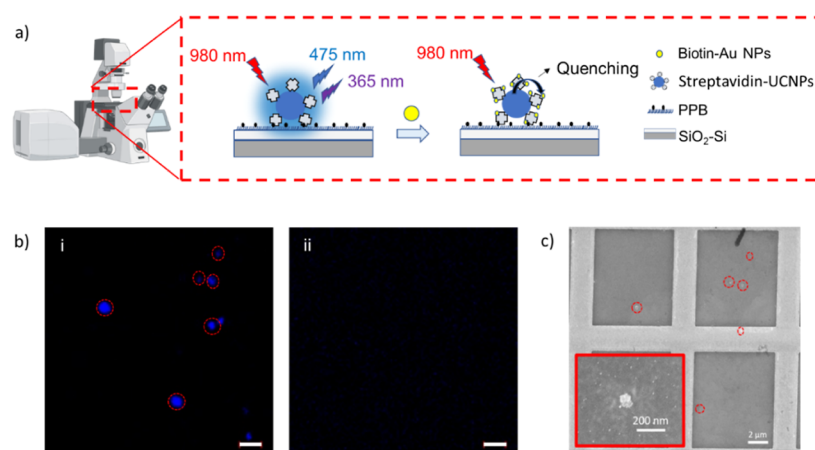


Figure 2. Validation of FRET between SA-UCNPs and biotin-AuNPs based on a commercial fluorescence microscope. (a) Schematic of the FRET process between SA-UCNPs and biotin-AuNPs. The microscope schematic was created using BioRender.com. (b) Fluorescence images of SA-UCNPs before (left) and after (right) incorporating biotin-AuNPs, scale bars: 2 μm . (c) Top-view SEM image of the same area as in (b) after adding biotin-AuNPs and then washing where the zoom-in lower-left frame marked with the red rectangle shows several AuNPs conjugated on a single UCNP.

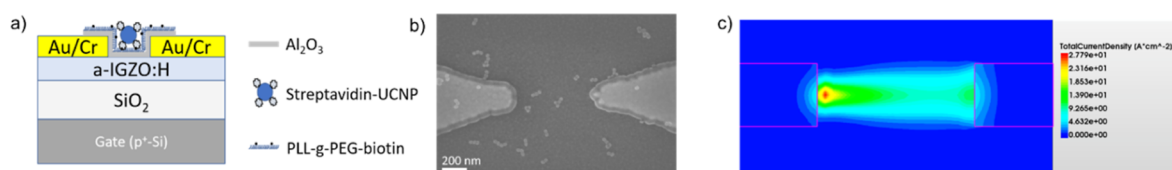


Figure 3. Characterization of IGZO:H-TFTs. (a) Schematic cross-section of an IGZO:H-TFT with an SA-UCNP immobilized on top of the Al_2O_3 layer between the source and drain electrodes after surface functionalization. (b) Top-view SEM image of a fabricated device after dispersing UCNPs. (c) Top-view current contour between the source and drain electrodes in (b) by TCAD simulation.

demonstrated by first turning them “ON” with the UV-blue lights from the immobilized SA-UCNPs and then turning them “OFF” by quenching the SA-UCNPs via FRET with the addition of biotin-AuNPs. The following sections describe these steps in detail.

Validation of FRET between SA-UCNPs and biotin-AuNPs

The quenching effect of the biotin-AuNPs on the SA-UCNPs was confirmed by using a commercial scanning confocal fluorescence microscope. The experiments were carried out on a silicon wafer with a 100 nm thick thermally grown SiO_2 layer, see Figure 2a. To immobilize the SA-UCNPs, the SiO_2 surface was functionalized with biotinylated poly(L-lysine)-grafted-poly(ethylene glycol) (PPB) copolymer via electrostatic interaction. The poly ethylene glycol (PEG) in the PPB monolayer reduces the nonspecific adsorption of other proteins,⁴⁰ while the PPB monolayer itself specifically captures the SA-UCNPs through the well-known biotin–streptavidin coupling. Upon excitation by a 980 nm pulsed laser, the immobilized SA-UCNPs on the surface emitted strong blue and violet lights; see Figure 2b(i). The fluorescence from SA-UCNPs was completely quenched after adding biotin-AuNPs that are about 2 nm in diameter; see Figure 2b(ii). To further confirm that the disappearance of fluorescent signals is due to quenching rather than other effects, imaging under a scanning electron microscope of the same area was performed after fluorescence imaging. The SEM image of the SA-UCNPs (Figure 2c) correlates well with the fluorescence image [Figure 2b(i)], which validates the success of surface functionalization and subsequent immobilization of SA-UCNPs. A zoomed-in image even reveals the biotin-AuNPs captured on a single SA-UCNP, lower-left frame in Figure 2c. The quenching effect of

biotin-AuNPs on SA-UCNPs agrees with other published reports and is due to the FRET process between the SA-UCNPs and biotin-AuNPs.^{41,42} The streptavidin–biotin pair brings the UCNPs and AuNPs close and the wide absorption spectrum of the AuNPs overlaps with the emission peaks of the UCNPs.^{41,42}

Fabrication of IGZO:H-TFTs and Integration with Colloidal SA-UCNPs

Sensor chips featuring arrayed IGZO:H-TFTs were designed and fabricated based on silicon technology. A schematic of the device structure is shown in Figure 3a. Details of the fabrication are presented in the section Device Fabrication. To increase the stability of the electrical performance of the phototransistors for measurements both in air and in liquid, a 30 nm thick Al_2O_3 passivation layer was grown by means of atomic layer deposition (ALD) on top of the α -IGZO:H film (see Figure S1).^{43,44} An IGZO:H-TFT with a channel of 500 nm in length and 500 nm in width, defined by the dimensions of the source and drain electrodes, was first measured in the dark. It is characterized by a maximum on-to-off current ratio ($I_{\text{on}}/I_{\text{off}}$) of 10^9 , subthreshold swing (SS) of 0.3 V/decade, threshold voltage (V_{th}) of +2.0 V, and saturation mobility (μ_{sat}) of $31.3 \text{ cm}^2/(\text{V s})$ (see Figure S2).^{23–25} The large SS and V_{th} values mainly result from the very thick back SiO_2 gate dielectric used.⁴⁵

To immobilize the colloidal SA-UCNPs on top of the IGZO:H-TFT channel, the surface of the Al_2O_3 passivation layer was functionalized with PPB. The colloidal SA-UCNPs were subsequently captured onto the functionalized Al_2O_3 surface above the channel region between the source and drain electrodes, see Figure 3a,b. Some UCNPs were found

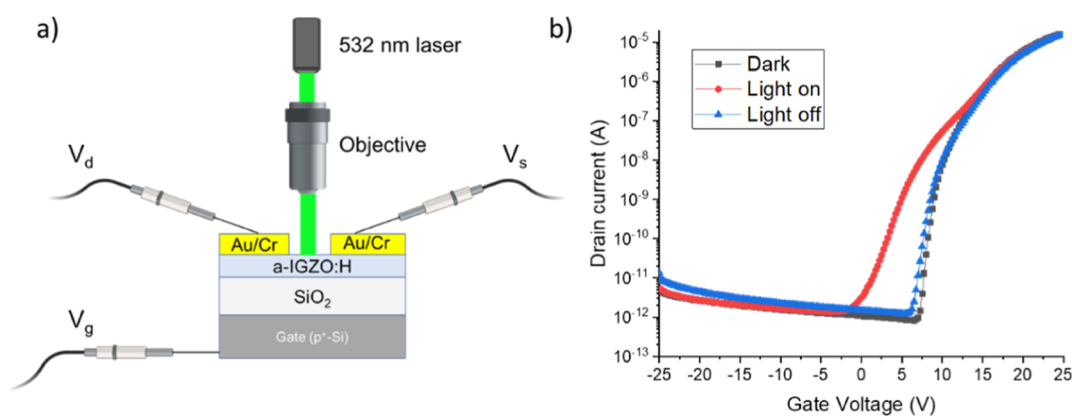


Figure 4. Photoresponse of the IGZO:H-TFTs. (a) Schematic of an IGZO:H-TFT measured on a probe station with the irradiation of 532 nm light. The schematics of probes, the objective, and the laser source were created using BioRender.com. (b) Transfer characteristics of the IGZO:H-TFT measured in air in the dark (black curve), under a 532 nm CW laser irradiation (red curve), and after turning off the light (blue curve), all at source-drain voltage $V_d = 10$ V.

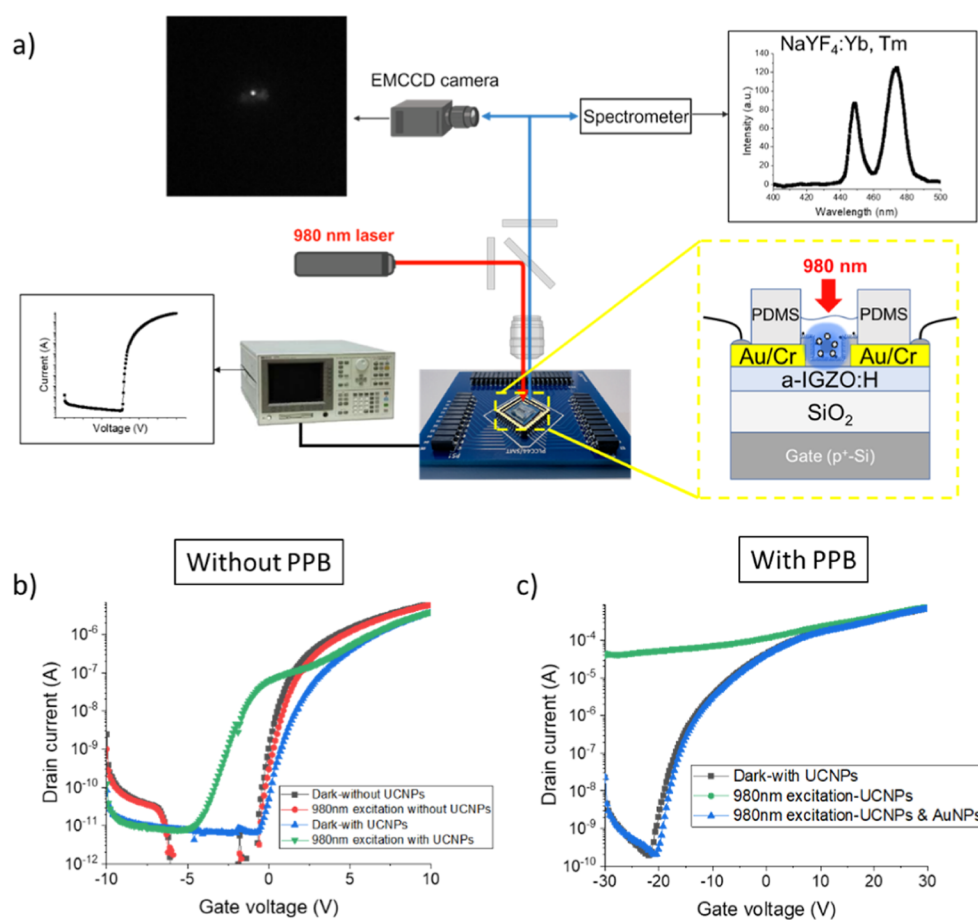


Figure 5. (a) Schematic of the integrated optoelectronic measurement setup including a μ PL microscope-based optical system and electrical measurement setup. The schematics of the 980 nm laser, mirrors, the objective, and the EMCCD were created using BioRender.com. The IGZO:H-TFT sensor chip is wire-bonded onto a chip carrier soldered on a custom-designed PCB. Photoresponse of IGZO:H-TFTs. (b) Transfer characteristics of an IGZO:H-TFT without PPB functionalization at different steps to show the integration of IGZO:H-TFT with UCNPs. (c) Transfer characteristics of a different IGZO:H-TFT yet of identical geometry with that in (b) but with PPB functionalization to demonstrate the entire process including incorporation of biotin-AuNPs as the final step. The devices were measured both in dark and under 980 nm light illumination.

along the periphery of the channel area, and they could also be excited due to the large size of the incident laser spot with a Gaussian distribution in intensity ($\sim 30 \mu\text{m}$ in diameter). As the α -IGZO:H thin film was not etched into well-defined

channels for the TFTs, a concern thus arises from the potential contribution of the UCNPs lying outside the effective channel area defined by the region in between the electrodes (see Figure 3b). We, therefore, performed TCAD simulation of the

current distribution between the source and drain electrodes of an IGZO:H-TFT with a gap distance of 500 nm in length and 200 nm in width (Figure 3c). The simulation shows that the current flows between the source and drain with very limited side spread, i.e., the current density decays exponentially from the central line of the channel to the outside (in perpendicular to the current flow direction). Specifically, it drops to 1/e of its highest value along the central line of the channel at around 100 nm away. The fraction of the current flowing outside this border only amounts to maximumly 37% of the total current. Therefore, the emitted light from the UCNP's lying 100 nm away from this central line would have a negligible contribution to the photocurrent by also considering the near-zero radiation angle between the α -IGZO:H film and the outlying UCNP's.

FRET Characterization on IGZO:H-TFTs

The photoresponse of the IGZO:H-TFT without UCNP's was first investigated by irradiating an IGZO:H-TFT directly with a 532 nm green diode laser on the probe station hosting the chip; see Figure 4a. The measured transfer characteristics (i.e., drain current I_{DS} vs gate voltage V_G) of the device confirm the visible-light detection capability of the IGZO:H-TFT, see Figure 4b.

The PCB-mounted chips with immobilized SA-UCNP's were subsequently characterized using a semiconductor parameter analyzer and a microphotoluminescence (μ PL) system (see Figure 5a and the Optoelectronic Characterization section for details). For measurements in liquid, a PDMS container was mounted on top of the chip. The μ PL system was used to align the laser spot with the transistor channel and verify the fluorescence signals of the UCNP's by the EMCCD camera and the spectrometer during the measurements. All transfer characteristics were measured at a constant $V_D = 10$ V to put the device in its saturation mode, see Figure S2.

As expected, excitation by the 980 nm laser does not generate any photocurrent in the IGZO:H-TFT in the absence of UCNP's (red curve in comparison to black curve in Figure 5b). After immobilization of SA-UCNP's but measured in the dark, appreciable modifications of the transfer characteristics are observed (blue curve in comparison to black curve in Figure 5b). These modifications are likely caused by surface adsorption of ions in the electrolyte carrying the SA-UCNP's, thereby altering the surface potential of the IGZO:H-TFT. Upon excitation with the 980 nm NIR CW laser, the UCNP's emit ultraviolet and blue light causing an anticipated negative shift of V_{th} (green curve in comparison to the blue curve in Figure 5b). The successful operation of the integrated UCNP's-IGZO:H-TFT yet with a limited response prompted the characterization of the entire concept. Thus, after surface functionalization with PPB to enhance the immobilization of SA-UCNP's, another (yet geometrically identical) IGZO:H-TFT shows a much stronger photoresponse when illuminated with the 980 nm NIR CW laser; the off-state branch of the transfer characteristics below $V_G = 0$ V is substantially raised from its reference level obtained without illumination (green curve in comparison to black curve in Figure 5c). This raised branch falls back to the original level when biotin-AuNP's are drop-casted to the chip surface (blue curve in comparison with black curve in Figure 5c), thereby not only validating the FRET-based quenching effect but also proving the concept of high-specificity detection based on the sensor setup in Figure 5a.

Photoconductive and photogating effects can generate the photocurrent of phototransistors.^{32,43} The former refers to the photocurrent increase due to the increased channel conductivity by photogenerated excess carriers. The latter is typically manifested with a V_{th} shift caused by the photogenerated carriers being trapped in localized states or present at the interface between the gate insulator and the channel, as illustrated by the band diagram of the device in Figure S3. The device in Figure 5b without the PPB functionalization has fewer UCNP's than those on the device in Figure 5c (Figure S4). As a result, lower visible light intensity is expected for the device in Figure 5b, resulting in generation of fewer electron-hole pairs (EHP's) sufficient for the observed V_{th} shift, i.e., the photogating effect dominates. For the device in Figure 5c with a larger number of UCNP's due to the PPB surface functionalization generating a significantly larger concentration of EHP's, the channel conductivity is also enhanced in addition to a V_{th} shift, i.e., the photoconductive effect governs. The initial V_{th} difference between the two IGZO:H-TFT's in Figure 5b,c is possibly due to the positive charge of PPB.⁴⁶ Different times and intensities of the unavoidable white light-emitting diode illumination while aligning the 980 nm laser beam with the channel may also affect.³⁶

Figures of merit of the IGZO:H-TFT's can be calculated in accordance with the equations below

$$PR = \frac{I_{light} - I_{dark}}{\frac{A_{W \times L}}{P}} \frac{1}{A_{spot}} \quad (1)$$

$$PS = \frac{I_{light} - I_{dark}}{I_{dark}} \quad (2)$$

$$D^* = \frac{PR}{\sqrt{2q}J_{dark}} \quad (3)$$

where, PR, PS, and D^* represent photoresponsivity, photo-sensitivity, and detectivity, respectively.³⁶ $A_{W \times L}$ is the IGZO channel size (300 \times 1000 nm) between the source and drain electrodes of the device in Figure 5c, P the incident laser power density, A_{spot} the laser spot area, J_{dark} the dark current density, and q the elemental charge. It is assumed that the shot noise from the dark current dominates while calculating D^* . The calculation shows that the IGZO:H-TFT with UCNP and PPB is characterized by PR = 54.2 mA/W, PS = 10^5 , and $D^* = 9.6 \times 10^6$ Jones at a gate voltage biased at -25 V with a power density of 980 nm laser about 4×10^3 W/cm² according to Figure 5c. These parameters are highly dependent on the number of UCNP's between the source and drain electrodes. Usually, a dense layer of UCNP's is combined with photo-detectors to increase their spectral response.⁹⁻²⁰ However, for a photodetector-based biosensor with high sensitivity, only a few UCNP's or even a single UCNP is desired as a bioreceptor between the source and drain. Therefore, these parameters are incomparable with those from reports using a dense layer of UCNP's. In our work here, around 100 UCNP's were found to remain between the source and drain electrodes of the IGZO:H-TFT after the optoelectronic measurements in Figure 5c (see Figure S4). Hence, it is reasonable to estimate that each UCNP may have a photocurrent-to-dark current ratio of $\sim 10^3$. Furthermore, each UCNP could at most capture ~ 100 biotin-AuNP's and complete the quenching (Figure 2c). Thus, each biotin-AuNP may cause at least 1 order of magnitude

decrease of the photocurrent, thereby holding promises for single molecule detection.

The UCNPs were photostable. We measured the PL intensity of a single UCNP over a 100 s duration, and it was photostable without displaying any tendency of photobleaching, see Figure S5d. The optoelectronic measurement was performed 1 day after loading the UCNPs on the chip, validating that the UCNPs and the IGZO:H TFTs were stable for storage for at least 24 h. However, it is challenging to reuse them after adding AuNPs to the container. Regeneration of the devices can be desirable, but it lies outside our focus here. Regarding repeatability, the IGZO:H TFTs from different batches (the ones in Figures 5b–c, S1 and S2) had similar transfer curves measured in the dark without UCNPs. Moreover, the PPB on the surface of Al₂O₃ is judged uniform, which was indicated by the satisfactorily uniform SA-UCNPs on the PPB-functionalized Al₂O₃ surface in a larger view, see Figure S6. However, it should be noted that the number of UCNPs between the source and drain electrodes can vary due to aggregation of UCNPs, preparation of the UCNP solution, and the way of sample loading. The optical response of the device is sensitive to the number of UCNPs between the source and drain electrodes.

For ultimate single-molecule detection, selective surface functionalization could be combined with nanostructures to site-specifically immobilize a single UCNP per phototransistor. The UCNP and FRET-based detection can be further applied for various analytes such as ions, DNA, or proteins with this setup in the future. Other photodetectors, which detect visible light but not NIR light, can also be used for the integration with UCNPs and FRET for molecular detection. For application scenarios such as a portable sensing device, a 980 nm CW diode laser with sufficient power density, a microfluidic system for analyte delivery, and an integrated circuit for supplying and processing electrical signals can be integrated with our phototransistor chip.

CONCLUSIONS

A novel highly sensitive optoelectronic sensor chip featuring an α -IGZO:H-based TFT photodetector has been realized. The concept combines FRET-assisted quenching of fluorescence from upconversion nanocrystals to design a compact yet highly scalable optoelectronic molecular sensor. The IGZO:H-TFTs with submicrometer channel size and visible light detection ability were designed and fabricated with standard silicon technology. Colloidal SA-UCNPs were drop-casted and immobilized on the TFT-channel after functionalizing the Al₂O₃-passivated channel with PPB. A high ratio of photocurrent to dark current was achieved at a negative gate bias under 980 nm NIR light illumination due to the unique anti-Stokes shift property of the UCNPs. Biotin-AuNPs were shown to completely quench the emission of SA-UCNPs via FRET. The FRET-based quenching effect was confirmed by the sharp photocurrent drop of the IGZO:H-TFT.

METHODS

Fluorescence Imaging of UCNPs on the SiO₂–Si Substrate

To facilitate navigation and focus under the microscope, gold grid markers with a thickness of 40 nm were first fabricated on a thermally oxidized silicon substrate featuring a 150 nm thick oxide layer. These markers were produced by using electron-beam lithography (EBL), followed by evaporation and lift-off processes. Subsequently, the substrate underwent an oxygen plasma treatment for surface

functionalization. A custom-made PDMS container with a diameter of 7 mm was used to apply 100 μ L of 1 mg/mL PLL-g-PEG-biotin onto the substrate. Then, 100 μ L of 20 μ g/mL SA-UCNPs (NaYF₄, Yb: Tm@NaYF₄, Ruixibiotech, China) was added to the PDMS container and incubated for 1 h to immobilize the SA-UCNPs. These SA-UCNPs are core–shell type nanoparticles, with diameters ranging from 30 to 40 nm, an excitation peak at 980 nm, and emission peaks centered at 365 and 470 nm (see Figure S5). After thorough washing with 1 \times phosphate-buffered saline and drying with nitrogen gas, the single SA-UCNPs were characterized using a commercial scanning confocal-based multiphoton microscope (Zeiss LSM 710) equipped with a mode-locked Ti/sapphire pulsed laser (Mai Tai HP, 80 MHz repetition rate and <100 fs pulse width). Fluorescence images of the SA-UCNPs were taken in the same area on the substrate, guided by the gold grid markers, both before and after the addition of biotin-AuNPs. After a 30 min incubation period, the unbound AuNPs were washed away with deionized (DI) water. Imaging parameters included a 20 \times /1.0 NA objective, 5.85 mW average laser power, 21 \times 21 μ m scanning area, 208 \times 208 pixels resolution, 9.5 s/frame, averaging over 4 frames, main beam splitter at 760, 371–500 nm emission filter, and a photomultiplier photodetector with 10 \times digital gain.

Device Fabrication

The fabrication of TFTs with staggered-type α -IGZO:H channels began with the thermal oxidation of p⁺-silicon substrate wafers, resulting in a 120 nm thick SiO₂ layer as the gate insulator. The substrate functioned as the back gate following oxide etching from the backside and the sputtering of a 100 nm thick aluminum layer to form the back-contact. A 40 nm thick α -IGZO film was then sputter-deposited in Ar/H₂ plasma to create the α -IGZO:H layer on the front side of the wafers.³⁶ Next, a bilayer structure consisting of a 5 nm thick Cr adhesion layer and a 40 nm thick Au metallization layer was patterned as the source and drain electrodes on top of the α -IGZO:H layer using EBL, evaporation, and lift-off processes. Specifically, the PMMA-A4 electron resist (MicroChem, Germany) was spin-coated at 6000 rpm and soft-baked at 180 °C. EBL (nB5, NanoBeam, UK) with a 2 nA current and 80 kV accelerating voltage was utilized to write patterns for the source and drain electrodes. The pattern was developed in a 1:3 mixture of methyl isobutyl ketone (EMD Millipore, Germany) and isopropanol for 40 s, then rinsed in DI water for 1 min. Sequential evaporation of a 5 nm thick Cr film and a 40 nm thick Au film was conducted by electron beam evaporation (Kurt J. Lesker PVD 75, Germany), followed by a lift-off process in a heated acetone bath.

To create signal lines and large contact pads for wire bonding, UV-5 resist (0.8, Microresist, Germany) was used for a second EBL step to reduce writing time due to its much lower dose requirement compared to that of PMMA resist. After exposure and development in MF-CD26 solution (SPEC EM, Switzerland) for 70 s, the Cr/Au evaporation and lift-off processes were repeated. To protect device performance from moisture or oxygen and mitigate leakage between the α -IGZO:H layer and liquids during subsequent electrical characterization in electrolytes, a 30 nm thick Al₂O₃ passivation layer was deposited on top of the channel region, electrodes, and metallization leads using ALD (Picosun R200, Finland) at 180 °C with a glass shadow mask. The fabricated chip was wire-bonded onto a chip carrier (LCC04420, Spectrum, United States) that was presoldered onto a custom-designed PCB. Wire bonding was manually executed with Au wires and silver paste (Sigma-Aldrich, Sweden).

TCAD Simulation

The current distribution (Figure 2c) was simulated by using the Synopsys Sentaurus three-dimensional TCAD simulation tool. The IGZO material was approximated by using n-doped silicon with an electron concentration of 10¹⁶ cm⁻³.^{47,48} Ideal ohmic contacts were assumed, with a source-drain voltage of 10 V and a gate voltage of 0 V.

Optoelectronic Characterization

The fabricated IGZO:H-TFTs were first tested for visible light responsiveness using a 532 nm green diode laser mounted on a semiconductor probe station, supported by a B1500A semiconductor analyzer (Keysight, United States).

The chip on a PCB connecting a semiconductor parameter analyzer (Hewlett-Packard 4155A, United States) was integrated with a μ PL microscope system (Zeiss Axio Observer Z1, Germany) comprising a 980 nm CW laser (Thorlabs, L980P030, United States), a thermoelectrically cooled EMCCD camera (Andor iXon3 888, Northern Ireland), and a spectrometer (Andor SR500, Northern Ireland) to facilitate optoelectronic characterization of the TFTs in electrolytes. A short-pass 720 nm emission filter (Semrock, FF01-720/SP-25) was utilized before the EMCCD. A 100 \times /0.73 NA air objective (Nikon, Japan) was employed to focus the laser beam on the chip in bright-field mode with a power density of approximately 4 \times 10³ W/cm² to both excite the UCNP and collect photoluminescence signals. The gate voltage for the TFTs swept from -30 to +30 V with a fixed source-drain voltage of 10 V. The SA-UCNP solution was diluted in DI water and drop-casted onto the chip in a custom-made PDMS container.

ASSOCIATED CONTENT

Supporting Information

The Supporting Information is available free of charge at <https://pubs.acs.org/doi/10.1021/acsaoam.4c00310>.

Additional optoelectronic measurements, information on the UCNP, and schematics of the device (PDF)

AUTHOR INFORMATION

Corresponding Author

Shi-Li Zhang – Division of Solid-State Electronics, Department of Electrical Engineering, The Ångström Laboratory, Uppsala University, SE-751 03 Uppsala, Sweden; orcid.org/0000-0003-2417-274X; Email: shili.zhang@angstrom.uu.se

Authors

Yupeng Yang – Division of Solid-State Electronics, Department of Electrical Engineering, The Ångström Laboratory, Uppsala University, SE-751 03 Uppsala, Sweden; orcid.org/0000-0003-1623-1615

Mohammad Hadi Khaksaran – Division of Solid-State Electronics, Department of Electrical Engineering, The Ångström Laboratory, Uppsala University, SE-751 03 Uppsala, Sweden; orcid.org/0000-0002-2404-1769

Jong Bin An – School of Electrical and Electronic Engineering, Yonsei University, KR-037 22 Seoul, Republic of Korea

Sujin Lee – School of Electrical and Electronic Engineering, Yonsei University, KR-037 22 Seoul, Republic of Korea

Hyun Jae Kim – School of Electrical and Electronic Engineering, Yonsei University, KR-037 22 Seoul, Republic of Korea; orcid.org/0000-0002-6879-9256

Ted Johansson – Division of Solid-State Electronics, Department of Electrical Engineering, The Ångström Laboratory, Uppsala University, SE-751 03 Uppsala, Sweden

Xi Lu – Department of Applied Physics, School of Engineering Sciences, KTH Royal Institute of Technology, SE-100 44 Stockholm, Sweden

Ilya Sychugov – Department of Applied Physics, School of Engineering Sciences, KTH Royal Institute of Technology, SE-100 44 Stockholm, Sweden; orcid.org/0000-0003-2562-0540

Apurba Dev – Division of Solid-State Electronics, Department of Electrical Engineering, The Ångström Laboratory, Uppsala University, SE-751 03 Uppsala, Sweden; Department of Applied Physics, School of Engineering Sciences, KTH Royal Institute of Technology, SE-100 44 Stockholm, Sweden; orcid.org/0000-0002-6235-2891

Complete contact information is available at: <https://pubs.acs.org/10.1021/acsaoam.4c00310>

Author Contributions

S.-L.Z. conceived the idea. Y.Y. conducted the major part of the work under the supervision of S.-L.Z. and A.D. Y.Y., S.-L.Z., and H.J.K. designed the α -IGZO devices, A.J.B., S.L., and H.J.K. prepared the α -IGZO:H bare films on SiO₂-p⁺-Si substrates, and Y.Y. fabricated the devices. T.J. did the electric simulation of the device. Y.Y. and M.H.K. designed the PCB circuits and optimized the wire bonding. Y.Y. did the fluorescence imaging with the assistance of X.L. and S.I.. Y.Y. did the optoelectronic measurements of the fabricated phototransistors. All authors contributed to the analysis of the experimental and theoretical data. Y.Y. and S.-L.Z. wrote the manuscript with input from M.H.K., X.L., T.J., A.D., S.I., A.J.B., S.L., and H.J.K.

Notes

The authors declare no competing financial interest.

ACKNOWLEDGMENTS

This work was sponsored by the Swedish Research Council (2018-03494). We acknowledge Myfab Uppsala for providing facilities and experimental support. Myfab is funded by the Swedish Research Council (2019-00207) as a national research infrastructure.

REFERENCES

- Haase, M.; Schäfer, H. Upconverting Nanoparticles. *Angew. Chem., Int. Ed.* **2011**, *50* (26), 5808–5829.
- Hao, S.; Chen, G.; Yang, C. Sensing Using Rare-Earth-Doped Upconversion Nanoparticles. *Theranostics* **2013**, *3* (5), 331–345.
- Zheng, W.; Huang, P.; Tu, D.; Ma, E.; Zhu, H.; Chen, X. Lanthanide-Doped Upconversion Nano-Bioprobes: Electronic Structures, Optical Properties, and Biodetection. *Chem. Soc. Rev.* **2015**, *44* (6), 1379–1415.
- Wang, F.; Banerjee, D.; Liu, Y.; Chen, X.; Liu, X. Upconversion Nanoparticles in Biological Labeling, Imaging, and Therapy. *Analyst* **2010**, *135* (8), 1839–1854.
- DaCosta, M. V.; Doughan, S.; Han, Y.; Krull, U. J. Lanthanide Upconversion Nanoparticles and Applications in Bioassays and Bioimaging: A Review. *Anal. Chim. Acta* **2014**, *832*, 1–33.
- Zhou, J.; Liu, Q.; Feng, W.; Sun, Y.; Li, F. Upconversion Luminescent Materials: Advances and Applications. *Chem. Rev.* **2015**, *115* (1), 395–465.
- König, K. Multiphoton microscopy in life sciences. *J. Microsc.* **2000**, *200*, 83–104.
- Williams, R. M.; Zipfel, W. R.; Webb, W. W. Multiphoton Microscopy in Biological Research. *Curr. Opin. Chem. Biol.* **2001**, *5* (5), 603–608.
- Kataria, M.; Yadav, K.; Haider, G.; Liao, Y. M.; Liou, Y. R.; Cai, S. Y.; Lin, H. L.; Chen, Y. H.; Inbaraj, C. R. P.; Bera, K. P.; Lee, H. M.; Chen, Y. T.; Wang, W. H.; Chen, Y. F. Transparent, Wearable, Broadband, and Highly Sensitive Upconversion Nanoparticles and Graphene-Based Hybrid Photodetectors. *ACS Photonics* **2018**, *5* (6), 2336–2347.
- Thakur, M. K.; Gupta, A.; Fakhri, M. Y.; Chen, R. S.; Wu, C. T.; Lin, K. H.; Chattopadhyay, S. Optically Coupled Engineered

Upconversion Nanoparticles and Graphene for a High Responsivity Broadband Photodetector. *Nanoscale* **2019**, *11* (19), 9716–9725.

(11) Wu, J.; Yang, Z.; Qiu, C.; Zhang, Y.; Wu, Z.; Yang, J.; Lu, Y.; Li, J.; Yang, D.; Hao, R.; Li, E.; Yu, G.; Lin, S. Enhanced Performance of a Graphene/GaAs Self-Driven Near-Infrared Photodetector with Upconversion Nanoparticles. *Nanoscale* **2018**, *10* (17), 8023–8030.

(12) Zhou, N.; Xu, B.; Gan, L.; Zhang, J.; Han, J.; Zhai, T. Narrowband Spectrally Selective Near-Infrared Photodetector Based on Up-Conversion Nanoparticles Used in a 2D Hybrid Device. *J. Mater. Chem. C* **2017**, *5*, 1591–1595.

(13) Zhai, Y.; Zhou, Y.; Yang, X.; Wang, F.; Ye, W.; Zhu, X.; She, D.; Lu, W. D.; Han, S. T. Near Infrared Neuromorphic Computing via Upconversion-Mediated Optogenetics. *Nano Energy* **2020**, *67*, 104262.

(14) Ghosh, S.; Chiang, W. C.; Fakhri, M. Y.; Wu, C. T.; Chen, R. S.; Chattopadhyay, S. Ultrasensitive Broadband Photodetector Using Electrostatically Conjugated MoS₂-Upconversion Nanoparticle Nanocomposite. *Nano Energy* **2020**, *67*, 104258.

(15) Zhang, Y.; Wang, J.; Wang, B.; Shao, J.; Deng, J.; Cong, C.; Hu, L.; Tian, P.; Liu, R.; Zhang, S.-L.; Qiu, Z. J. Extending the Spectral Responsivity of MoS₂ Phototransistors by Incorporating Up-Conversion Microcrystals. *Adv. Opt. Mater.* **2018**, *6*, 1800660.

(16) Yan, C.; Dadvand, A.; Rosei, F.; Perepichka, D. F. Near-IR Photoresponse in New Up-Converting CdSe/NaYF₄: Yb, Er Nanoheterostructures. *J. Am. Chem. Soc.* **2010**, *132* (26), 8868–8869.

(17) Li, J.; Shen, Y.; Liu, Y.; Shi, F.; Ren, X.; Niu, T.; Zhao, K.; Liu, S. F. Stable High-Performance Flexible Photodetector Based on Upconversion Nanoparticles/Perovskite Microarrays Composite. *ACS Appl. Mater. Interfaces* **2017**, *9* (22), 19176–19183.

(18) Ji, Y. N.; Zhou, D.; Wang, N.; Ding, N.; Xu, W.; Song, H. Flexible Double Narrowband Near-Infrared Photodetector Based on PMMA/Core-Shell Upconversion Nanoparticle Composites. *J. Rare Earths* **2022**, *40* (2), 211–217.

(19) Niu, W.; Su, L. T.; Chen, R.; Chen, H.; Wang, Y.; Palaniappan, A.; Sun, H.; Tok, A. I. Y. 3-Dimensional Photonic Crystal Surface Enhanced Upconversion Emission for Improved Near-Infrared Photoresponse. *Nanoscale* **2014**, *6*, 817–824.

(20) Xiang, H.; Zhou, L.; Lin, H. J.; Hu, Z.; Zhao, N.; Chen, Z. Upconversion Nanoparticles Extending the Spectral Sensitivity of Silicon Photodetectors to $\lambda = 1.5 \mu\text{m}$. *Nanotechnology* **2020**, *31* (49), 495201.

(21) Li, X.; Wei, L.; Pan, L.; Yi, Z.; Wang, X.; Ye, Z.; Xiao, L.; Li, H. W.; Wang, J. Homogeneous Immunosorbent Assay Based on Single-Particle Enumeration Using Upconversion Nanoparticles for the Sensitive Detection of Cancer Biomarkers. *Anal. Chem.* **2018**, *90* (7), 4807–4814.

(22) Ansari, A. A.; Thakur, V. K.; Chen, G. Functionalized Upconversion Nanoparticles: New Strategy Towards FRET-Based Luminescence Bio-Sensing. *Coord. Chem. Rev.* **2021**, *436*, 213821.

(23) Nomura, K.; Ohta, H.; Takagi, A.; Kamiya, T.; Hirano, M.; Hosono, H. Room-Temperature Fabrication of Transparent Flexible Thin-Film Transistors Using Amorphous Oxide Semiconductors. *Nature* **2004**, *432*, 488–492.

(24) Kamiya, T.; Nomura, K.; Hosono, H. Present Status of Amorphous In–Ga–Zn–O Thin-Film Transistors. *Sci. Technol. Adv. Mater.* **2010**, *11* (4), 044305.

(25) Kamiya, T.; Hosono, H. Material Characteristics and Applications of Transparent Amorphous Oxide Semiconductors. *NPG Asia Mater.* **2010**, *2*, 15–22.

(26) Zhu, Y.; He, Y.; Jiang, S.; Zhu, L.; Chen, C.; Wan, Q. Indium–Gallium–Zinc–Oxide Thin-Film Transistors: Materials, Devices, and Applications. *J. Semicond.* **2021**, *42* (3), 031101.

(27) Shi, J.; Zhang, J.; Yang, L.; Qu, M.; Qi, D. C.; Zhang, K. H. L. Wide Bandgap Oxide Semiconductors: from Materials Physics to Optoelectronic Devices. *Adv. Mater.* **2021**, *33*, 2006230.

(28) Song, J.; Huang, X.; Han, C.; Yu, Y.; Su, Y.; Lai, P. Recent Developments of Flexible InGaZnO Thin-Film Transistors. *Phys. Status Solidi A* **2021**, *218*, 2000527.

(29) Jeon, Y.; Lee, D.; Yoo, H. Recent Advances in Metal-Oxide Thin-Film Transistors: Flexible/Stretchable Devices, Integrated Circuits, Biosensors, and Neuromorphic Applications. *Coatings* **2022**, *12* (2), 204.

(30) Rim, Y. S. Review of Metal Oxide Semiconductors-Based Thin-Film Transistors for Point-of-Care Sensor Applications. *J. Inf. Dispers. Technol.* **2020**, *21* (4), 203–210.

(31) Takechi, K.; Iwamatsu, S. Sensor Applications of InGaZnO Thin-Film Transistors. *Jpn. J. Appl. Phys.* **2019**, *58*, 090504.

(32) Yoo, H.; Lee, I. S.; Jung, S.; Rho, S. M.; Kang, B. H.; Kim, H. J. A Review of Phototransistors Using Metal Oxide Semiconductors: Research Progress and Future Directions. *Adv. Mater.* **2021**, *33*, 2006091.

(33) Chen, S.; Zhang, S.-L. Contacting Versus Insulated Gate Electrode for Si Nanoribbon Field-Effect Sensors Operating in Electrolyte. *Anal. Chem.* **2011**, *83* (24), 9546–9551.

(34) Stern, E.; Wagner, R.; Sigworth, F. J.; Breaker, R.; Fahmy, T. M.; Reed, M. A. Importance of the Debye Screening Length on Nanowire Field Effect Transistor Sensors. *Nano Lett.* **2007**, *7* (11), 3405–3409.

(35) Abliz, A.; Wang, J.; Xu, L.; Wan, D.; Liao, L.; Ye, C.; Liu, C.; Jiang, C.; Chen, H.; Guo, T. Boost Up the Electrical Performance of InGaZnO Thin Film Transistors by Inserting an Ultrathin InGaZnO:H Layer. *Appl. Phys. Lett.* **2016**, *108*, 213501.

(36) Kang, B. H.; Kim, W. G.; Chung, J.; Lee, J. H.; Kim, H. J. Simple Hydrogen Plasma Doping Process of Amorphous Indium Gallium Zinc Oxide-Based Phototransistors for Visible Light Detection. *ACS Appl. Mater. Interfaces* **2018**, *10* (8), 7223–7230.

(37) Wang, X. L.; Shao, Y.; Wu, X.; Zhang, M. N.; Li, L.; Liu, W. J.; Zhang, D. W.; Ding, S. J. Light Response Behaviors of Amorphous In–Ga–Zn–O Thin-Film Transistors via In Situ Interfacial Hydrogen Doping Modulation. *RSC Adv.* **2020**, *10*, 3572–3578.

(38) Abliz, A. Effects of Hydrogen Plasma Treatment on the Electrical Performances and Reliability of InGaZnO Thin-Film Transistors. *J. Alloys Compd.* **2020**, *831*, 154694.

(39) Rho, H. Y.; Bala, A.; Sen, A.; Jeong, U.; Shim, J.; Oh, J. O.; Ju, Y.; Naqi, M.; Kim, S. Plasma-Engineered Amorphous Metal Oxide Nanostructure-Based Low-Power Highly Responsive Phototransistor Array for Next-Generation Optoelectronics. *ACS Appl. Nano Mater.* **2023**, *6* (17), 15990–15999.

(40) Ruiz-Taylor, L. A.; Martin, T. L.; Zaugg, F. G.; Witte, K.; Indermuhle, P.; Nock, S.; Wagner, P. Monolayers of Derivatized Poly (L-Lysine)-Grafted Poly (Ethylene Glycol) on Metal Oxides as a Class of Biomolecular Interfaces. *Proc. Nat. Acad. Sci.* **2001**, *98* (3), 852–857.

(41) Mendez-Gonzalez, D.; Melle, S.; Calderón, O. G.; Laurenti, M.; Cabrera-Granado, E.; Egatz-Gómez, A.; López-Cabarcos, E.; Rubio-Retama, J.; Diaz, E. Control of Upconversion Luminescence by Gold Nanoparticle Size: from Quenching to Enhancement. *Nanoscale* **2019**, *11*, 13832–13844.

(42) Wang, L.; Yan, R.; Huo, Z.; Wang, L.; Zeng, J.; Bao, J.; Wang, X.; Peng, Q.; Li, Y. Fluorescence Resonant Energy Transfer Biosensor Based on Upconversion-Luminescent Nanoparticles. *Angew. Chem., Int. Ed.* **2005**, *44*, 6054–6057.

(43) Huang, S. Y.; Chang, T. C.; Chen, M. C.; Chen, T. C.; Jian, F. Y.; Chen, Y. C.; Huang, H. C.; Gan, D. S. Improvement in the Bias Stability of Amorphous InGaZnO TFTs Using an Al₂O₃ Passivation Layer. *Surf. Coat. Technol.* **2013**, *231*, 117–121.

(44) Corsino, D. C.; Bermundo, J. P. S.; Fujii, M. N.; Takahashi, K.; Ishikawa, Y.; Uraoka, Y. Dimethylaluminum Hydride for Atomic Layer Deposition of Al₂O₃ Passivation for Amorphous InGaZnO Thin-Film Transistors. *Appl. Phys. Express* **2018**, *11*, 061103.

(45) Sze, S. M.; Li, Y.; Ng, K. K. *Physics of Semiconductor Devices*; John Wiley & Sons, 2021.

(46) Takechi, K.; Nakata, M.; Azuma, K.; Yamaguchi, H.; Kaneko, S. Dual-Gate Characteristics of Amorphous InGaZnO₄ Thin-Film Transistors as Compared to Those of Hydrogenated Amorphous Silicon Thin-Film Transistors. *IEEE Trans. Electron Devices* **2009**, *56* (9), 2027–2033.

(47) Fung, T. C.; Chuang, C. S.; Chen, C.; Abe, K.; Cottle, R.; Townsend, M.; Kumomi, H.; Kanicki, J. Two-Dimensional Numerical Simulation of Radio Frequency Sputter Amorphous In–Ga–Zn–O Thin-Film Transistors. *J. Appl. Phys.* **2009**, *106*, 084511.

(48) Martins, J.; Barquinha, P.; Goes, J. TCAD Simulation of Amorphous Indium-Gallium-Zinc Oxide Thin-Film Transistors. In *Technological Innovation for Cyber-Physical Systems: 7th IFIP WG 5.5/SOCOLNET Advanced Doctoral Conference on iComputing, Electrical and Industrial Systems, DoCEIS 2016, Costa de Caparica, Portugal, April 11–13, 2016, Proceedings 7*; Springer International Publishing, 2016; pp 551–557.